Electrochemical corrosion performance of copper and uniformly alloyed bronze and brass in 0.1 M NaCl solution

A. Abdullah Khan[a], S. Kaiser[b] and M. Salim Kaiser[c,*]

[a]*Department of Mechanical Engineering, Bangladesh University of Engineering and Technology, Dhaka-1000, Bangladesh*

[b]*Department of Civil Engineering, Bangladesh University of Engineering and Technology, Dhaka-1000, Bangladesh*

[c]*Directorate of Advisory, Extension and Research Services, Bangladesh University of Engineering and Technology, Dhaka-1000, Bangladesh*

[*]*e-mail: mskaiser@iat.buet.ac.bd*

Received 18 December 2022; accepted 2 March 2023

The influence of Al and Zn by 10 wt.% as alloying elements on the electrochemical corrosion behaviour of Cu-based alloy in 0.1 M NaCl solution is examined. Results from both electrochemical impedance spectroscopy method and potentiodynamic techniques indicate that the corrosion occurred at a higher rate for Zn and Al added alloys than pure Cu, where Zn added alloy shows the worst corrosion performance. Copper forms a stable, protective layer of Cu_2O, and CuO, as a result, has a lower corrosion rate. In case of Al and Zn, added alloys, dealloying, as well as dissolution of additional Al_2O_3 and ZnO, are responsible for higher corrosion rates, respectively. The surfaces are investigated by optical and scanning electron microscopy. Phases of different intermetallics within the Cu matrix are identified in the etched optical micrographs of the experimental alloys. The optical images after corrosion depict layers of oxides on the surfaces where the Zn-added alloys are highly affected, followed by Al-added alloys and pure Cu. Increased amounts of internal damage to the surface of the Zn-added alloy are visible in the SEM images. The EDX spectrum not only supports the presence of oxide layers but also claims that Zn-containing particles are dissolved at a greater rate than Al.

Keywords: Cu-based alloys; impedance; EIS; Tafel; microstructure.

DOI: https://doi.org/10.31349/RevMexFis.69.051002

1. Introduction

Copper is employed in electrical wiring, electrical appliances, and heat exchangers. In marine applications, such as propellers and propeller shafts, aluminium bronze and high-strength brass are utilized [1]. For condensers in freshwater applications, brasses are generally occupied. Copper alloys are also utilized in numerous significant applications, for example, in water distribution systems, marine applications etc. [2, 3]. These alloys have very good resistance to corrosion, good strength, fatigue resistance and conductivity [4-7]. Corrosion is an important phenomenon to observe in metals, as it naturally degrades the metal surfaces exposed to environments containing oxygen. The process converts metals into a more stable form of oxides. As a result, not only the chemical but physical properties of an alloy are also affected by the corrosion process [8]. Although most of the structural alloys corrode by the moisture in the air, the process can be accelerated when exposed to certain other substances. Small amounts of alloying elements are frequently added to metals to upgrade their properties. A metal's strength, hardness, electrical and thermal conductivity, corrosion resistance, and colour can be changed to meet demand through alloying. The improvement of one feature by the addition of a substance may have unanticipated impacts on other properties. The precipitates of intermetallics are allocated into the microstructure in response to heat treatment. The alloying elements in copper play a vital role in both the strengthening effect and other properties like corrosion [9]. The chloride environment has an adverse corrosive effect on the alloy surface as Cl- ions promote pitting corrosion [10]. Moreover, Cl- ions accelerate the rate of dissolution of protective oxide layers. According to the literature, chloride solution exhibits a much higher rate of redissolution of the protective Cu2O layer than chloride-free solution [2, 11]. Electrochemical impedance spectroscopy is a useful method of characterizing electrochemical corrosion properties, such as diffusion rates, reactions etc. Although this approach is susceptible to potential interpretation problems, modelling with optimally fitted circuits can improve the understanding of electrochemical corrosion [12]. Again, the technique of potentiodynamic polarization is a generally acknowledged method for identifying localized corrosion caused by pitting corrosion.

Various investigations on the effect of alloying elements on the corrosion behaviour of alloys under corrosive medium are going on [13]. But few works are there studying the role of alloying elements on the corrosion performance of copper alloy under sodium chloride solution. This article evaluates the effect of alloy composition on the electrochemical corrosion behaviour of Al and Zn added Cu alloys under 0.1 M NaCl solution. Ten weight percentages of each alloying element are considered to identify the individual severity of corrosion. For the investigation of the corrosion behaviour, electrochemical techniques such as potentiodynamic polarization and electrochemical impedance spectroscopy (EIS), surface characterization, including optical microscopy, scanning electron microscopy (SEM) and energy dispersive spectroscopy (EDS) have been performed.

2. Experimental

Commercially pure Cu, Cu-10Al as Al-bronze and Cu-10Zn alloy as α-brass were utilized in this investigation. Aluminium, zinc, and commercially pure copper were melted, which was executed in a crucible of clay graphite in a pit furnace which is natural gas fired. The chemical compositions of the samples were obtained by optical emission spectroscopy (OES) method which are shown in Table I. The cast alloys were machined into $15 \times 20 \times 150$ mm^3. Then the alloys were cold-rolled using a laboratory-scale rolling mill by 40% reduction. The samples acquired from the cold rolling were of $9 \times 20 \times 20$ mm^3 size and were aged at 200°C for 60 min for attaining peak hardness and stress relieving [14]. To measure the hardness of the aged samples, a Zwick Rockwell hardness tester with a 1/8-inch ball was used on the B scale. Density was considered from the elemental composition of the alloys. Tensile test was carried out at 10^{-3} s^{-1} strain rate using an Instron testing machine according to ASTM. The samples were machined to produce working electrodes of $4 \times 5 \times 35$ mm^3 size. 4×5 mm^2 surfaces were exposed, while coating the remaining surface by PVC heat shrinkable tube. Afterwards, the exposed surfaces of the alloys were polished mechanically with emery papers of 320 to 2000 grits.

A 100 mL three-electrode glass cell was utilized for the electrochemical study. 0.585 g of analytical reagent grade sodium chloride powder was dissolved into 100 mL of deionized water to prepare the 0.1 M sodium chloride solution. The rectangular coated experimental samples were used as the working electrodes, a platinum electrode was considered as the counter electrode and an Ag|AgCl-KCl was used as the reference electrode. To prepare the three-electrode glass cell, all three electrodes were dipped into the NaCl solution, and the glass was sealed to isolate it from the environment.

2.1. Electrochemical impedance spectroscopy (EIS)

The electrodes were connected to the CH Instruments - Electrochemical Workstation by crocodile clips. The system was maintained for around 30 minutes to reach a steady state. To obtain the open circuit potential (OCP) values, the voltages between the working and reference electrodes were measured. 5 mV amplitude and 100 kHz to 0.2 Hz frequency range were set for the sinusoidal voltage. Then the impedances for this range of frequencies were measured by the potentiostat at the open circuit potential. The EIS data were obtained after 30 minutes of stabilization for each sample. These impedance data were fitted to the appropriate electrical circuit in the program EC-Lab-Analyst. The circuit used in this study is called the Randles circuit. By modelling with this circuit, the system characteristics like, $R_P =$ polarization resistance (Ω), $R_S =$ solution resistance (Ω), and $C_{p(\text{eff})} =$ electrochemical double-layer capacitance (μF) were obtained.

2.2. Potentiodynamic polarization technique

For potentiodynamic polarization analysis, the same experimental setup was used. The electrode potential was changed from -1 to $+1$ V with a scan rate of 0.5 mVs^{-1}, and the corresponding corrosion current was measured. The formula employed for finding out the corrosion rate is,

$$\text{Corrosion rate} = \frac{I_{\text{corr}} \times K \times EW}{\rho \times A}, \tag{1}$$

where, I_{corr} corrosion current (A), K the constant which defines the corrosion rate units in mm year^{-1}, where $K = 3272$ mm (A cm year)$^{-1}$ according to ASTM standard G 102), EW the equivalent weight (g/equivalent), ρ the density in (gcm^{-3}), and A the surface area in (cm^2).

The microstructural images of polished surfaces of the alloys prior to and after corrosion were captured by OPTIKA, a typical optical microscope. In the case of the conventional optical microstructure of the aged alloys, the surfaces were metallographically etched by a typically suggested copper etchant, one of ammonium hydroxide + hydrogen peroxide (3%) in a 1:1 ratio. The SEM and EDX investigations were carried out using a JEOL scanning electron microscope with an attached X-ray analyzer.

3. Results and discussion

3.1. Physical properties

The effects of Al and Zn content by 10 wt% each on the physical and mechanical properties of Cu, alloy experimental results are exposed in the following two charts. Figure 1 shows the physical properties of the alloys related to hardness and density at peak aged conditions. It is observable from the figure that, at peak aged conditions, both Cu-10Al and Cu-10Zn have higher hardness values than pure Cu. As solution strengthening occurs through the dissolved Zn and Al atoms in the alloys. As a result, α-brass and Al-bronze have higher hardness compared to Cu [15,16]. Again, Al-bronze has superior hardness to Zn-bearing α-brass. During age hardening, five stable intermetallics of Al and Cu are formed: Cu_9Al_4, Cu_3Al_2, Cu_4Al_3, CuAl and $CuAl_2$. Among them, two specials are Cu_9Al_4 and Cu_3Al_2, which cause higher hardness in the Cu-10Al alloy [17,18]. These stable intermetallic phases have been identified in Cu-Al alloys in several previous investigations [19-21]. When the concentration of Zn is below 35 wt.%, the phase of brass is α, which has a substitutional and disordered face-centred-cubic (fcc) structure. As a result, Cu-10Zn shows a single fcc state of α-phase with no

TABLE I. Chemical composition of copper samples (wt.%).

Alloy	Al	Zn	Pb	Sn	Fe	Ni	Si	Cu
Cu	0.001	0.000	0.010	0.004	0.033	0.001	0.000	Bal
Cu-10Al	9.460	0.047	0.088	0.017	0.154	0.004	0.004	Bal
Cu-10Zn	0.013	10.300	0.012	0.007	0.057	0.005	0.004	Bal

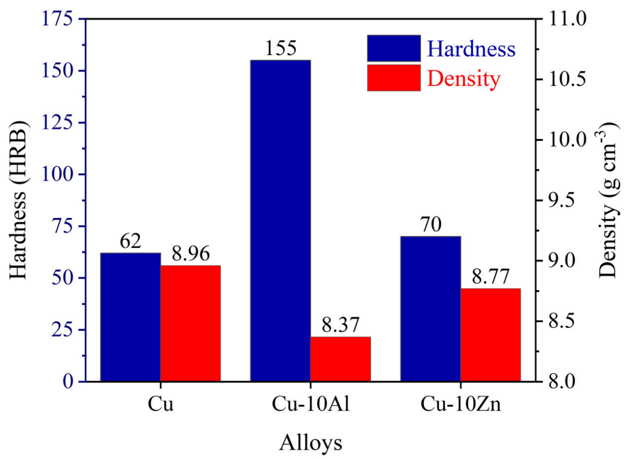

FIGURE 1. Variation of hardness and density of the pure Cu, Al and Zn added Cu alloys.

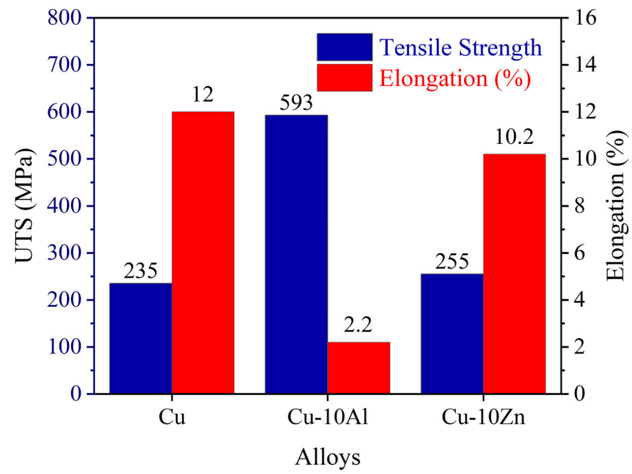

FIGURE 2.Variation of tensile strength and % elongation of the pure Cu, Al and Zn added Cu alloys.

discernible age-hardening effects, which makes Cu-10Zn alloy softer than Cu-10Al [22,23]. Additionally, in Fig. 1 depicts the variation of density among the experimental alloys. Pure copper has the highest density, whereas Al-bronze is the lightest, as the densities of Cu, Zn, and Al follow this sequence: Cu>Zn>Al. It can be seen from Table I. that Al and Zn are present in the alloys by 10 wt.%.

3.2. Mechanical properties

Figure 2 shows the mechanical properties of the pure copper, Al and Zn added Cu alloys in terms of tensile strength and % elongation. It is noted from the figure that both the Al-bronze (Cu-10Al) and the α-brass (Cu-10Zn) show better tensile strength but reduced ductility than Cu. Previous studies suggest that adding some alloying elements to copper improves tensile strength [24]. The results of the study support that zinc-added copper has more tensile strength and less % elongation than pure copper itself [25]. The higher content of zinc in Cu-10Zn increases brittleness [24]. The solid solution hardening of the α-phase of brass during the solidification process is responsible for this increased strength and reduced ductility. Again, the intermetallics formed during the solidification and ageing of Cu-10Al alloy, specially Cu_9Al_4 and Cu_3Al_2 intermetallics, increase the tensile strength and brittleness [17]. These precipitated particles hinder the dislocation movement, which leads to high tensile strength, but low ductility [18]. Furthermore, it is noticed from the figure that the Al added Cu has higher tensile strength and lower ductility than Cu-10Zn. The solid solution strengthening of Zn added Cu is not more prominent than Al added Cu alloy since Al-bronze consists of different intermetallics.

3.3. Impedance spectroscopy studies

The impedances were generated for variable frequencies between 100 kHz to 0.2 Hz by the potentiostat, CH Instruments - Electrochemical Workstation. The impedances were modeled with the electrical circuit in Fig. 3 to get the values of corresponding circuit components. The circuit components are solution resistance R_S, polarization resistance R_P, which is equivalent to charge transfer resistance R_{ct} [26], and effective double layer capacitance $C_{p(\text{eff})}$, the values of which are presented in Table II for the respective alloys. X^2 denotes the chi-squared value of goodness of fit. It has been previously found that the polarization resistance changes inversely with

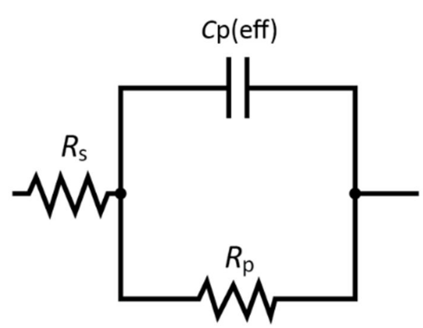

FIGURE 3. The equivalent electrical circuit for the impedance data.

TABLE II. Open circuit potential (OCP) values and electrochemical impedance spectroscopy (EIS) test results.

Alloy	OCP, V vs. SCE	Rp/Ω	Rs/Ω	$C_{p(\text{eff})}/\mu$F	X^2
Cu	-0.12913	26633	53.84	40.56	0.07667
Cu-10Al	-0.17519	18473	45.01	54.1	0.01711
Cu-10Zn	-0.20251	16192	36.48	83.66	0.00179

the corrosion rate of a metal, indicating the reactivity rate of the surface with the environment [27,28]. The R_P and R_{ct} are equivalent as they both indicate corrosion resistance.

From Table II, the observed phenomenon is that the OCP shifts towards a negative direction as alloying elements are added into the Cu, but the open circuit potential value of Zn added Cu alloy falls below Al added Cu alloy. The more positive open circuit potential expresses better corrosion resistance of metal [29]. Again, R_P is higher for pure copper rather than Al and Zn added alloys, and α-brass has the lowest value of R_P. This trend suggests that α-brass has the lowest corrosion resistance, while pure copper has the best corrosion protection among them. The addition of Al and Zn degrades the corrosion performance of Cu alloy as dealloying of Cu-Al and Cu-Zn occurs on the alloy surfaces due to the selective dissolution of Al and Zn. Moreover, the Cu-Zn solid solution is more prone to dealloying than Cu-Al solid solutions, which is why Zn-added α-brass shows the worst corrosion resistance [30]. Normally Al-bronze and α-brass are involved to produce a compact film composed of Al_2O_3 and ZnO along with Cu_2O, where Al-related oxide is more stable than that of Zn [30,31]. Pure copper shows the best performance as Cu is susceptible to forming cuprous oxide (Cu_2O) protective layer or to dope the film with the alloying elements' ions such as iron, and each of the experimental alloys has a trace amount of iron in it [32-34]. Copper, when immersed in NaCl solution, forms Cu_2O by this reaction [32,35]:

$$\mathrm{O_2} + 2\mathrm{H_2}O + 4\mathrm{e}^- \rightarrow 4\mathrm{OH}^-, \quad (2)$$

$$\mathrm{Cu} \rightarrow \mathrm{Cu}^+ + \mathrm{e}^-, \quad (3)$$

$$\mathrm{Cu}^+ 2\mathrm{Cl}^- \rightarrow \mathrm{CuCl}_2^-, \quad (4)$$

$$2\mathrm{CuCl_2} + 2\mathrm{OH}^- \rightarrow \mathrm{Cu_2O} + \mathrm{H_2O} + 4\mathrm{Cl}^-. \quad (5)$$

But, when Cu bonds with Al and Zn to produce solid solution strengthening and age hardening particles, they do not let Cu to easily form oxide. Zn forms a zinc hydroxy chloride ($Zn_5(OH)_8Cl_2$) surface film by the following reaction [36]:

$$\mathrm{Zn}(s) + \mathrm{Cl}^- + \mathrm{H_2O} \rightarrow \mathrm{Zn_2(OH)_8Cl_2}(f). \quad (6)$$

Again, Assaf, *et al.* [36], investigated that passive zinc oxide film is formed by the following reaction:

$$\mathrm{Zn} + (\mathrm{OH})^-(\mathrm{ads}) \rightarrow \mathrm{ZnO} + \mathrm{H}^+ + 2\mathrm{e}^-. \quad (7)$$

The aluminium oxide formation is shown in the equation below [37]:

$$2\mathrm{Al} + 3\mathrm{H_2}O \rightarrow \mathrm{Al_2O_3} + 3\mathrm{H_2}. \quad (8)$$

However, the values of R_s show a decreasing trend from Cu to Al and Zn added alloys in the table, and $C_{p(\text{eff})}$ shows the opposite trend. As Rs dominates the total path resistance, it follows a similar trend as R_p [38].

Figure 4 displays the Nyquist diagram for the copper alloys. This diagram follows the capacitive-resistive semicircle model, which provides the real (Zr) and imaginary (Zi) parts of the impedances, respectively. The charge transfer process regulates the electrochemical corrosion of pure copper and copper alloys, as indicated by a full semicircular shape on the Nyquist diagram [39].

The Bode magnitude and phase plots are shown in Figs. 5a) and b), respectively. At the y-axis of the Bode magnitude plot, the modulus of impedance ($|Z|/\Omega$) is presented, whereas the negative values of phase angles ($-\varphi/°$) are denoted at the y-axis of the Bode phase plot. On the other hand, the x-axes of both the Bode magnitude and phase plots denote the frequency (f/Hz). The impedance can be determined by the following equation:

$$Z(\omega) = R_s + \frac{R_p}{1 + j\omega R_p C_d}. \quad (9)$$

From the equation, it is known that at high frequency, the right term of the equation gets close to zero, and the

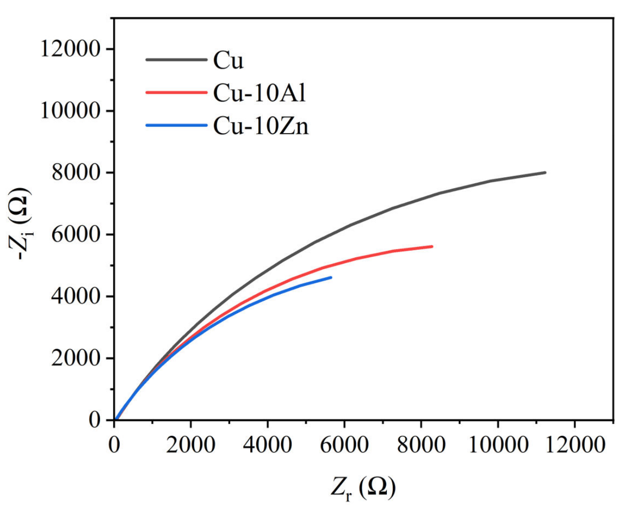

FIGURE 4. Nyquist diagram for the pure Cu, Al and Zn added Cu alloys.

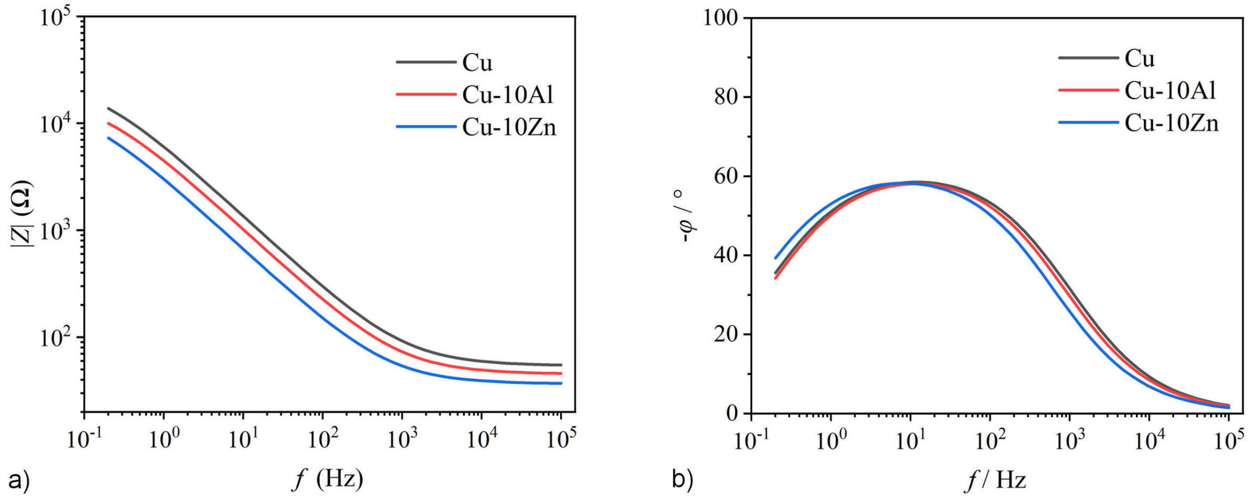

FIGURE 5. Bode a) magnitude, and b) phase diagrams of the pure Cu, Al and Zn added Cu alloys.

impedance is close to the solution resistance. Figure 5a) shows a similar trend. The Bode magnitude plot for pure Cu is situated higher than Al-bronze, where the curve for α-brass lies lower than the alloy with a higher amount of Al, which can be explained by Eq. (6) and Table II. From the table, both R_s and R_p are higher in Al-bronze than α-brass, the pure Cu having the maximum value. For higher values of R_s and R_p, the impedance must be higher, according to Eq. (5). In Fig. 5b), no phase shift is there at lower and higher frequencies, indicating a resistive response. On the other hand, at mid-range frequencies, the phase shifts are closer to $-90°$, which is a capacitive response.

3.4. Potentiodynamic polarization analysis

Figure 6 shows the potentiodynamic polarization curves obtained under scan rate of 0.5 mVs^{-1} applying electrode potentials from -1 V to $+1$ V, for the commercially pure Cu,

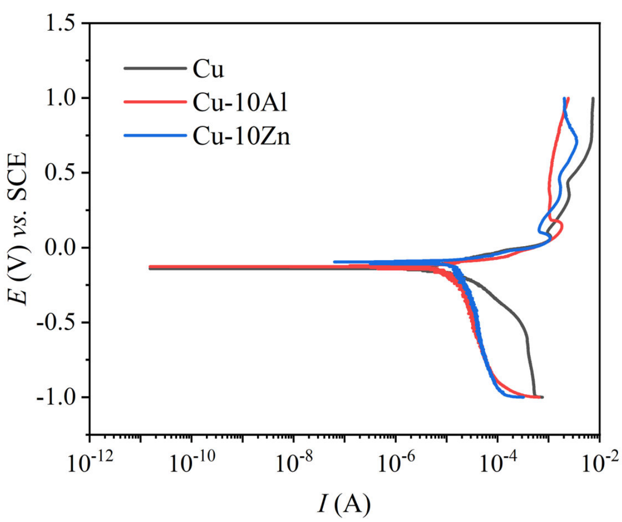

FIGURE 6. Tafel polarization curves for the pure Cu, Al and Zn added Cu alloys.

TABLE III. Corrosion parameters obtained from potentiodynamic polarization analysis.

Alloy	I_{corr}/μA	E_{corr}/mV	Corrosion rate, mm/year
Cu	2.86	-140.3	0.1659
Cu-10Al	7.99	-126.98	0.4627
Cu-10Zn	11.31	-95.28	0.6720

Al added Cu alloy as Al-bronze, and Zn added Cu alloy as α-brass. The experimental results of the potentiodynamic polarization analyses obtained through Eq. (1) are furnished in Table III. The corrosion current is expressed by I_{corr}, the corrosion potential or rest potential is expressed by E_{corr}, and the corrosion rate is denoted in mm/year unit. Inspecting the Tafel plots, it is noticed that the slope of the curve for pure Cu is higher than the other two curves for the Zn and Al-added Cu alloys. The higher the slope, the slower the corrosion should take place, as the change in corrosion current is smaller [40].

The experimental data suggest that the corrosion current and corrosion rate are higher in Al, and Zn added alloys, where Zn added alloy showing the maximum corrosion. This can be interpreted as the pure copper exhibits the best corrosion resistance, whereas the α-brass depicting the worst resistance followed by Al-bronze, which behavior is like the EIS analysis.

3.5. Optical micrographic observation

Figure 7 presents the optical micrographs of Cu, Cu-10Al and Cu-10Zn alloys prior to and post corrosion process in 0.1 M NaCl solution. The surfaces of the alloys were highly polished with emery papers for getting smooth surfaces. There are slight scratches due to polishing. Although not very much difference can be observed from this type of unetched microstructures, but as there were different alloying elements

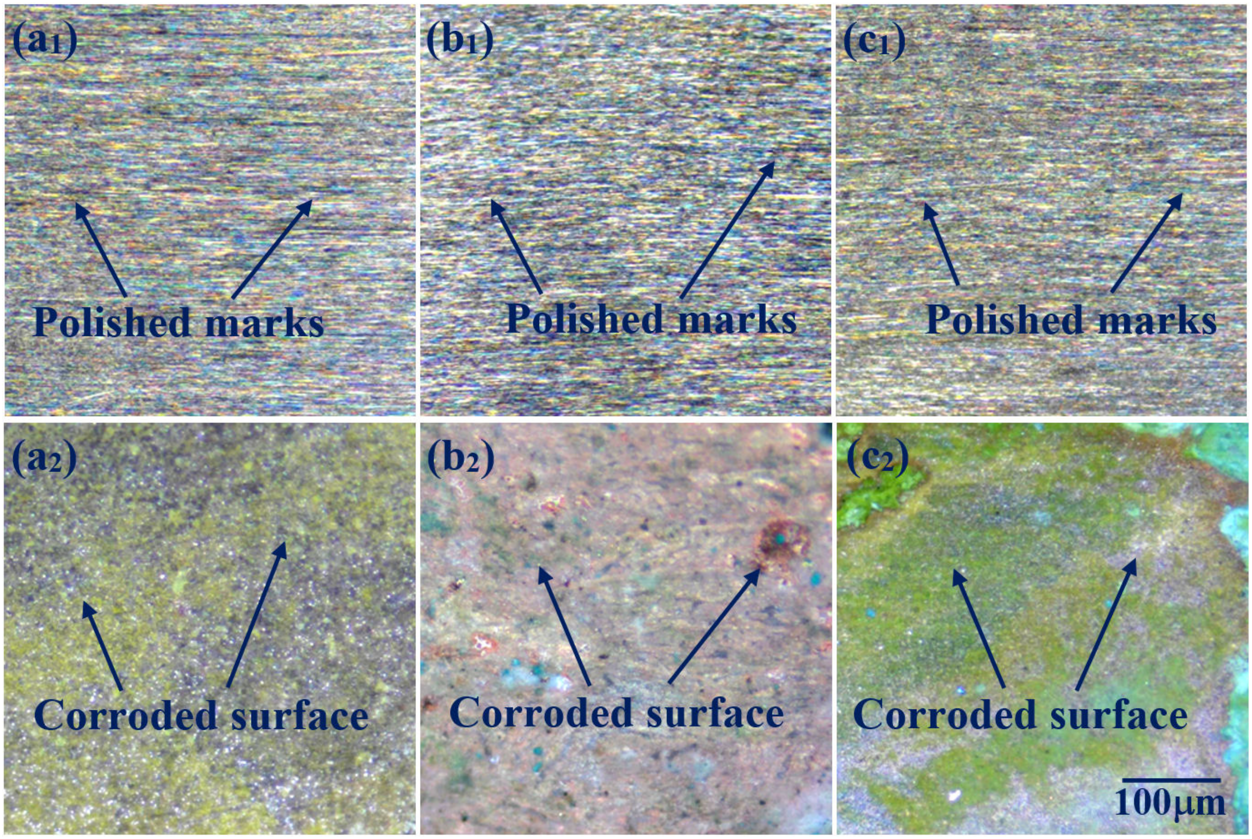

FIGURE 7. Optical micrographic images of the surfaces of pure Cu, Al and Zn added Cu alloys before and after corrosion in 0.1 M NaCl solution.

present, a varied tone can be detected in the alloys. Pure copper shows orange-tinted red, Al-bronze exhibits dull gold tones, and α-brass shows reddish gold before corrosion in Figs. 7a1) to 7c1). Again, some differences are discernible among the micrographs of the metal surfaces after corrosion in Figs. 7a2) to 7c2) and no polished marks are visible. A uniformly distributed corroded surface is found in Fig. 7a2), as there is no intermetallic formed in pure copper. However, different intermetallics of copper aluminates associated with trace impurities cause localized pitting corrosion in Cu-10Al alloy, which can be observed in Fig. 7b2) [41]. Figure 7c2) shows an extensive amount of pitting corrosion caused by the Zn solid solution, as well as trace impurities into the matrix and the preferential dissolution in the case of Cu-10Zn alloy [42]. As Cu and Zn have a large difference in equilibrium potential difference, selective dissolution of Zn occurs. It has been previously inspected that both physical and surface phases were remarkably changed due to anodic dissolution or free corrosion of brass [43]. In the micrographs of corroded surfaces, pure copper is turned into yellow and green colour as typical of Cu_2O and CuO, which is visible in Fig. 7a2) [44].

There is a film of Al_2O_3 on the surface of Cu-10Al in Fig. 7b2), which is white in general. The ZnO together with CuO shows the white and green tone on the surface of Cu-10Zn alloy in Fig. 7c2) [45]. The micrographs also display the highest damaged surface of the Zn added alloys and followed by Al-added alloys and then pure Cu. These results also comply with the experimental results of the corrosion rate of the experimental alloys.

The conventional optical microstructures of the etched pure Cu, Al and Zn added Cu alloys are shown in Fig. 8, after cold rolling and peak aged conditions. Due to rolling by 40% deformation, elongated and broken grains are formed in the direction of rolling. The grains become elongated in the direction of the applied stress, irreversibly changing the microstructure during cold working. The distribution of the size of the Cu grains is not uniform, and there are some smaller grains visible in the middle of the coarse grains, where several twins also exist within the grains [Fig.8a)] [46]. Different phases such as α-phase, several κ-phases, and retained β' phase are there in Al-bronze. The specific phases also refine the grain structure [47]. Cu-Zn alloy shows a single-phase fcc condition because the level of Zn content is below 35 wt.%. The single-phase brass is formed when Zn is melted into Cu and develops a uniform crystal structure, revealed by the Cu-10Zn alloy's resultant microstructures [Fig. 8c)]. Similar observations are also made by the earlier investigators [48].

3.6. SEM and EDX observation

The surface micrographs of the corroded surfaces of the pure Cu, Al-bronze and α-brass using SEM are presented in Fig. 9.

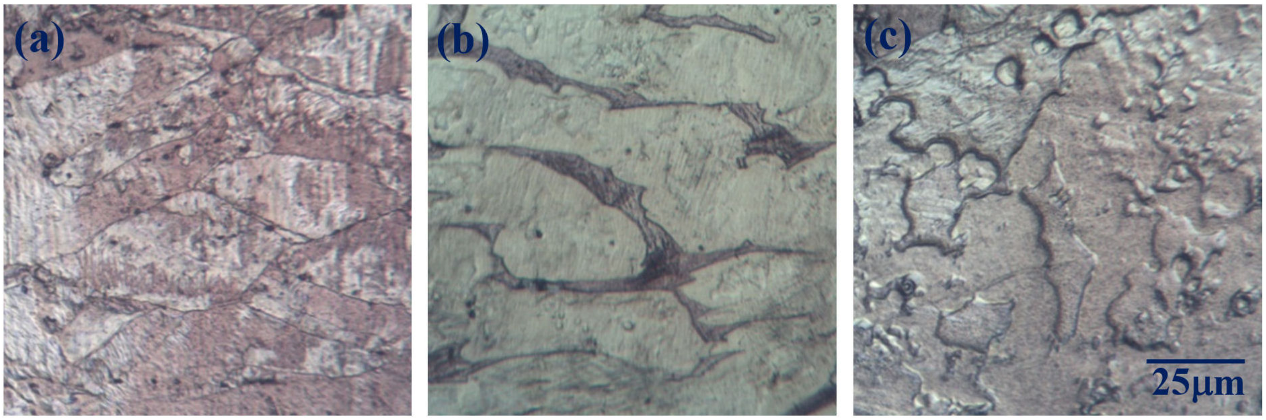

FIGURE 8. Optical microstructures of the etched samples of pure Cu, Al and Zn added Cu alloys.

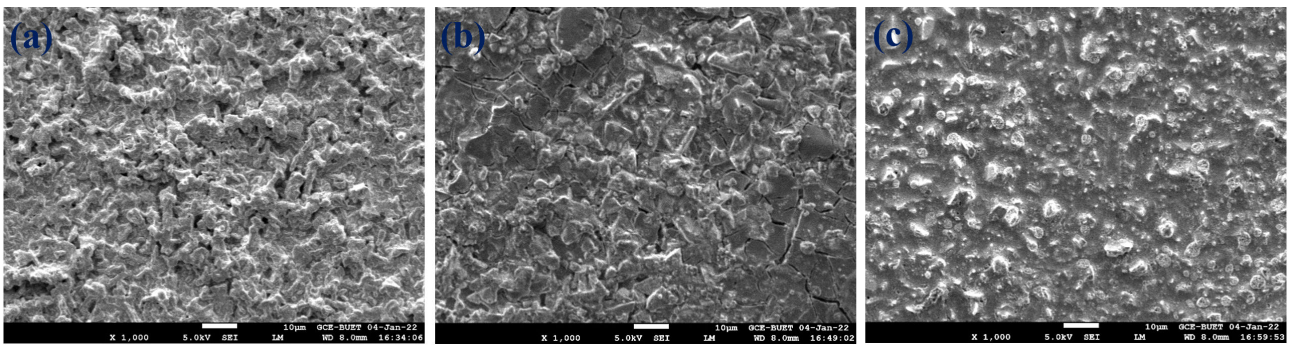

FIGURE 9. SEM images of a) pure Cu, b) Al added Cu, c) Zn added Cu alloys after corrosion in 0.1 M sodium chloride medium.

TABLE IV. EDX analysis of corroded surface of the alloys.

Alloy	Content, wt.%						
	Cu	O	Al	Zn	Fe	Na	Cl
Pure Cu	46.74	23.67	0.00	0.00	0.00	0.00	29.59
Cu-10 Al	45.02	15.43	5.45	0.00	0.76	0.00	33.34
Cu-10 Zn	44.99	24.89	0.05	1.61	0.38	0.30	27.78

The uneven surface topography is visible due to the formation and demolishment of oxide layers for each sample. It is conspicuous that the dissolution of pure copper is homogeneous, which is depicted in Fig. 9a), whereas there is selective dissolution in the case of Al-added Cu and Zn-added Cu in Figs. 9b) and c). Furthermore, surface defects such as microcracks and pinholes are visible, which are, to a greater extent, on the surfaces of Al and Zn-added Cu alloys. The pinholes are the effects of pitting corrosion which seems excessively on the surface of Cu-10Zn alloy, caused by the Cu-Zn solid solution matrix and the preferential dissolution as discussed previously. One significant observation is that Zn bearing alloy surface shows thick oxide layers with internal massive damage. The pitting potentials in Cu-Al and Cu-Zn alloys are higher than in pure copper, which may be due to the presence of the mixed passive films Cu_2O and Al_2O_3 in Cu-Al alloy and Cu_2O and ZnO in Cu-Zn alloy [30,31]. The dissolution rate of oxide film ZnO is higher and not too stable than that of Al_2O_3.

According to the quantitative EDX analysis as tabulated in Table IV, the alloys show following chemical compositions in wt.%:

The compositions can be interpreted as the wt.% of Al is reduced from 9.46% to 5.45% in Al-bronze after corrosion. On the other hand, the wt.% of Zn is reduced during corrosion from 10.3% to 1.61%, depicting that dissolution of Zn bearing particles in α-brass is more prominent than Al bearing particles in Al-bronze. During the corrosion process, the element Zn and Al unalloyed form the α-brass and Al-bronze, which dissolved easily. As a result, such lower levels of Zn remain in the alloy. The percentages of oxygen in every alloy indicate the layers of oxides formed.

4. Conclusions

Corrosion of copper along with Al and Zn added alloys in 0.1M NaCl solution has been successfully investigated. The main conclusions of the experimental results can be summarized as follows:

- Among the three samples, pure copper has shown the highest corrosion resistance, whereas Zn added α-brass showing the lowest, followed by Al-bronze, by both EIS and Tafel analyses. This is because the Cu-Zn solid solution is more prone to dealloying than Cu-Al solid solutions, and pure Cu serves homogeneous corrosion protection by forming different oxide layers of copper.

- As the surfaces deteriorate, the polished marks are removed, which can be observed in the optical microstructures. A variation in colour tones can also be observed in the different alloys, both before and after corrosion. More pinholes can be observed because of pitting corrosion and dealloying in the Zn alloyed sample than in the Al alloyed sample. Selective dissolution of Zn from the Cu-Zn alloy compared to Al from the Cu-Al alloy has occurred to a greater extent as Cu and Zn have a larger difference in equilibrium potential than Cu and Al. Micro cracks and pinholes are evidence of selective dissolution of alloy phases, which can be identified in the SEM images. The etched microstructures before corrosion exhibit different phases of α, β, β' and κ.

- The EDX spectra prove the presence of oxide layers on the surfaces after corrosion, and the degree of dissolution of Zn and Al added particles is higher in α-brass and Al-bronze. It also shows that the film of Al_2O_3 serves better protection than ZnO.

Acknowledgments

Thanks to the Department of Chemistry and DAERS office of Bangladesh University of Engineering and Technology, Dhaka-1000, for providing the laboratory facilities.

Conflict of interest

The authors would like to declare that there is no conflict of interest regarding this publication.

Funding

No external funding is received.

1. J. A. Wharton *et al.*, The corrosion of nickel-aluminium bronze in seawater, *Corrosion Science*, **47** (2005) 3336-3367. https://doi.org/10.1016/j.corsci.2005.05.053.
2. K. Ding, L. Fan, M. Yu, W. Guo, J. Hou and C. Lin, Sea water corrosion behaviour of T2 and 12832 copper alloy materials in different sea areas, Corrosion Engineering, *Science and Technology*, **54** (2019) 476-484, https://doi.org/10.1080/1478422X.2019.1619289.
3. Taher, Corrosion Behavior of Copper-Nickel Alloy in Marine Environment (Review Paper). *Applied Mechanics and Materials*, **799-800** (2015) 222-231, https://doi.org/10.4028/www.scientific.net/amm.799-800.222.
4. D. E. Tyler and W. T. Black, Introduction to Copper and Copper Alloys, ASM International, Materials Park, Ohio, USA, 1990.
5. S. Li, M. Fang, Z. Xiao, X. Meng, Q. Lei and Y. Jia, Effect of Cr addition on corrosion behavior of cupronickel alloy in 3.5 wt% NaCl solution, *Journal of Materials Research and Technology*, **22** (2023) 2222-2238, https://doi.org/10.1016/j.jmrt.2022.12.079.
6. A. H. Tuthill, Guidelines for the Use of Copper Alloys in Seawater, Nickel Development Institute, Ontario, Canada (1987).
7. J. A. Rogers, Dispersion-Strengthened Copper Alloys with Useful Electrical and Mechanical Properties, *Powder Metallurgy*, **20** (1977) 212-220. https://doi.org/10.1179/pom.1977.20.4.212.
8. G. Wang, R. Ma, M. Wan and F. Zhao, The Effect of Sr composition on the microstructure and mechanical properties of Al-Si-Zn filler for the brazing of AA6061, *Materials Research Express*, **9** (2022) 1-12. https://doi.org/10.1088/2053-1591/ac5776.
9. D. J. Horton, H. Ha, L. L. Foster, H. J. Bindig and J. R. Scully, Tarnishing and Cu Ion release in Selected Copper-Base Alloys: Implications towards Antimicrobial Functionality, *Electrochimica Acta*, **169** (2015) 351-366. https://doi.org/10.1016/j.electacta.2015.04.001.
10. D. Cicolin, M. Trueba and S. P. Trasatti, Effect of chloride concentration, pH and dissolved oxygen, on the repassivation of 6082-T6 Al alloy, *Electrochimica Acta*, **124** (2014) 27-35. https://doi.org/10.1016/j.electacta.2013.09.003.
11. D. D. Macdonald, Cyclic Voltammetry of Copper Metal in Lithium Hydroxide Solution at Elevated Temperatures, J*ournal of The Electrochemical Society*, **121** (1974) 651-656. https://doi.org/10.1002/Chin.197432035.
12. F. Ciucci, Modeling electrochemical impedance spectroscopy, *Current Opinion in Electrochemistry*, **13** (2019) 132-139. https://doi.org/10.1016/j.coelec.2018.12.003.
13. M. A. Nur, A. A. Khan, S. D. Sharma and M. S. Kaiser, Electrochemical corrosion performance of Si-doped Al-based automotive alloy in 0.1 M NaCl solution, *Journal of Electrochemical Science and Engineering*, **12** (2022) 565-576. https://doi.org/10.5599/jese.1373.

14. S. Kaiser and M. S. Kaiser, Wear Behavior of Commercial Pure Copper with Al and Zn under Dry, Wet and Corrosive Environment, *J. Mater. Environ. Sci.* **11** (2020) 551.

15. D. Zhang, Y. Li, K. Feng, P. Zhu and G. Xu, Effect of Aging Temperature on Microstructure and Mechanical Property of Aluminium Brass, IOP Conference Series: *Materials Science and Engineering*, **452** (2018) 1-5. https://doi.org/10.3139/146.11034010.1088/1757-899X/452/2/022132.

16. M. A. Bodude, I. Momohjimoh and R. N.Nnaji, Mechanical and Microstructural Evaluation of Plastically Deformed Brass, *Materials Sciences and Applications*, **6** (2015) 1137-1144. https://doi.org/10.4236/msa.2015.612112.

17. E. Altuncu, S. Iric and F. Ustel, Wear-resistant intermetallic arc spray coatings, *Materiali in Tehnologije*, **46** (2012) 181-183. https://hdl.handle.net/20.500.12619/49789.

18. M. Okayasu, T. Muranaga and A. Endo, Analysis of microstructural effects on mechanical properties of copper alloys", J*ournal of Science: Advanced Materials and Devices*, **2** (2017) 128-139. https://doi.org/10.1016/j.jsamd.2016.12.003.

19. K. Kim, D. Kim, K. Park, M. Cho, S. Cho and H. Kwon, Effect of Intermetallic Compounds on the Thermal and Mechanical Properties of Al-Cu Composite Materials Fabricated by Spark Plasma Sintering, *Materials (Basel)*, **12** (2019) 1-13, https://doi.org/10.3390/ma12091546.

20. L. Dong, W. Chen, L. Hou, Y. Liu and Q. Luo, Metallurgical process analysis and microstructure characterization of the bonding interface of QAl9-4 aluminum bronze and 304 stainless steel composite materials, *J. Mater. Process. Technol.* **238** (2016) 325-332, https://doi.org/10.1016/j.jmatprotec.2016.07.041.

21. D. Raju, A. R. Govindan, J. Subramanian, S. Ramachandran and S. Nair, Surface alloying of aluminium bronze with chromium: Processing, testing, and characterization, *Mater. Today Proc.* **27** (2020) 2191-2199, https://doi.org/10.1016/j.matpr.2019.09.094.

22. H. L. Hong, Q. Wang, C. Dong and P. K. Liaw, Understanding the Cu-Zn brass alloys using a short-range-order cluster model: significance of specific compositions of industrial alloys, Scientific Reports, **4** (2014) 1-4. https://doi.org/10.1038/srep07065.

23. A. Esmaeili, H. R. Zareie Rajani, M. Sharbati, M. K. B. Givi and M. Shamanian, The role of rotation speed on intermetallic compounds formation and mechanical behavior of friction stir welded brass/aluminum 1050 couple, *Intermetallics*, **19** (2011) 1711-1719, https://doi.org/10.1016/j.intermet.2011.07.006.

24. S. K. Jha, D. Balakumar and R. Paluchamy, Experimental analysis of microstructure and mechanical properties of copper and brass based alloys, *International Journal of Automotive and Mechanical Engineering*, **11** (2015) 2317-2331. https://doi.org/10.15282/ijame.11.2015.14.0195.

25. Z. Barlas and H. Uzun, Microstructure and mechanical properties of friction stir butt welded dissimilar pure copper/brass alloy plates, *International Journal of Materials Research*, **101** (2010) 801-807. https://doi.org/10.3139/146.110340.

26. S. A. R. Khan, M. A. Hossain, M. Al Nur and M. S. Kaiser, Electrochemical Corrosion Properties of Ternary Al and Quaternary Zr Added Bell Metal in 0.1M NaCl Solution, *Journal of Mechanical Engineering Science and Technology*, **5** (2021) 1-16. https://doi.org/10.17977/um016v5i12021p001.

27. S. Choudhary, A. Garg and K. Mondal, Relation between open circuit potential and polarization resistance with rust and corrosion monitoring of mild steel, *Journal of Materials Engineering and Performance*, **25** (2016) 2969-2976. https://doi.org/10.1007/s11665-016-2112-6.

28. J. Bessone, C. Mayer, K. Jüttner and W. J. Lorenz, AC-impedance measurements on aluminium barrier type oxide films, *Electrochimica Acta*, **28** (1983) 171-175. https://doi.org/10.1016/0013-4686(83)85105-6.

29. A. M. Alfantazi, T. M. Ahmed and D. Tromans, Corrosion behavior of copper alloys in chloride media, *Materials & Design*, **30** (2009) 2425-2430, https://doi.org/10.1016/j.matdes.2008.10.015.

30. B. G. Ateya, E. A. Ashour and S. M. Sayed, Stress Corrosion Behavior of α-Aluminum Bronze in Saline Water, *Corrosion*, **50** (1994) 20-25. https://doi.org/10.5006/1.3293490.

31. S. Virtanen, H. Wojtas, P. Schmuki and H. Böhni, Passivity of High Corrosion Resistant Cu-Al-Sn Alloys, *Journal of The Electrochemical Society*, **140** (1993) 2786-2790. https://doi.org/10.1149/1.2220911.

32. F. Mansfeld, G. Liu, H. Xiao, C. H. Tsai and B. J. Little, The corrosion behavior of copper alloys, stainless steels and titanium in seawater, *Corrosion Science*, **36** (1994) 2063-2095. https://doi.org/10.1016/0010-938X(94)90008-6.

33. R. F. North and M. J. Pryor, The influence of corrosion product structure on the corrosion rate of Cu-Ni alloys, *Corrosion Science*, **10** (1970) 297-311. https://doi.org/10.1016/S0010-938X(70)80022-1.

34. R. G. Blundy and M. J. Pryor, The potential dependence of reaction product composition on copper-nickel alloys, *Corrosion Science*, **12** (1972) 65-75. https://doi.org/10.1016/S0010-938X(72)90567-7.

35. A. Palit and S. O. Pehkonen, Copper corrosion in distribution systems: evaluation of a homogeneous Cu2O film and a natural corrosion scale as corrosion inhibitors, *Corrosion Science*, **42** (2000) 1801-1822, https://doi.org/10.1016/S0010-938X(00)00024-X.

36. S. Thomas, N. Birbilis, M. S. Venkatraman and I. S. Cole, Corrosion of Zinc as a Function of pH, *CORROSION*, **68** (2012) 1-9, https://doi.org/10.5006/1.3676630.

37. G. Scampone and G. Timelli, Anodizing Al-Si Foundry Alloys: A Critical Review, *Adv. Eng. Mater.* **24** (2022) 1-14, https://doi.org/10.1002/adem.202101480.

38. R. A. Buchanan and E. E. Stansbury, Electrochemical Corrosion, Handbook of Environmental Degradation of Materials, Elsevier, New York, USA (2005).

39. X. Li, S. Deng, H. Fu and G. Mu, Inhibition effect of 6-benzylaminopurine on the corrosion of cold rolled steel in H_2SO4 solution, *Corrosion Science*, **51** (2009) 620-634, https://doi.org/10.1016/j.corsci.2008.12.021.

40. S. S. Wang *et al.*, Effect of Cu Content and Aging Conditions on Pitting Corrosion Damage of 7xxx Series Aluminum Alloys, *Journal of The Electrochemical Society*, **162** (2015) 150-160. https://doi.org/10.1149/2.0301504jes.

41. R. G. Buchheit, L. P. Montes, M. A. Martinez, J. Michael and P. F. Hlava, The Electrochemical Characteristics of Bulk-Synthesized Al_2CuMg, *Journal of The Electrochemical Society*, **146** (1999) 4424-4428. https://doi.org/10.1149/1.1392654.

42. R. G. Buchheit, A Compilation of Corrosion Potentials Reported for Intermetallic Phases in Aluminum Alloys, *Journal of The Electrochemical Society*, **142** (1995) 3994-3996. https://doi.org/10.1149/1.2048447.

43. P. Zhou and K. Ogle, The Corrosion of Copper and Copper Alloys, in Encycl. Interfacial Chem., Elsevier, New York, USA (2018).

44. N. N. Greenwood and A. Earnshaw, Chemistry of the Elements, 2nd ed., Butterworth-Heinemann, Ed., Oxford, UK, (1997).

45. A. H. Battez *et al.*, CuO, ZrO2 and ZnO nanoparticles as antiwear additive in oil lubricants, *Wear*, **265** (2008) 422-428. https://doi.org/10.1016/j.wear.2007.11.013.

46. G. Purcek *et al*., Microstructure and mechanical behavior of UFG copper processed by ECAP following different processing regimes, *Philosophical Magazine*, **92** (2012) 690-704. https://doi.org/10.1080/14786435.2011.634842.

47. J. Hajek, A. Kriz, O. Chocholaty and D. Pakula, Effect of Heat Treatment on Microstructural Changes in Aluminium Bronze, *Archives of Metallurgy and Materials*, **61** (2016) 925-930. https://doi.org/10.1515/amm-2016-0210.

48. C. N. Panagopoulos, E. P. Georgiou and K. Simeonidis, Lubricated wear behavior of leaded $\alpha + \beta$ brass, *Tribology International*, **50** (2012) 1-5. https://doi.org/10.1016/j.triboint.2011.12.016.